Monitoring CO_2 intrusion and associated geochemical transformations in a shallow groundwater system using complex electrical methods

Baptiste Dafflon[1], Yuxin Wu[1], Susan S. Hubbard[1], Jens T. Birkholzer[1], Thomas M. Daley[1], John D. Pugh[2], John E. Peterson[1], and Robert C. Trautz[3]*

* Lawrence Berkeley National Laboratory (LBNL), 1 Cyclotron Rd., Berkeley, CA 94720, USA; Phone: 510-486-4735; e-mail: BDafflon@lbl.gov.

[1] Lawrence Berkeley National Laboratory (LBNL), 1 Cyclotron Rd., Berkeley, CA 94720, USA

[2] Southern Company Services, 600 N. 18th St., Birmingham, AL 35291, USA

[3] Electric Power Research Institute (EPRI), 3420 Hillview Avenue, Palo Alto, CA 94304, USA

ABSTRACT

The risk of CO_2 leakage from a properly permitted deep geologic storage facility is expected to be very low. However, if leakage occurs it could potentially impact potable groundwater quality. Dissolved CO_2 in groundwater decreases pH, which can mobilize naturally occurring trace metals commonly contained in aquifer sediments. Observing such processes requires adequate monitoring strategies. Here, we use laboratory and field experiments to explore the sensitivity of time-lapse complex resistivity responses for remotely monitoring dissolved CO_2 distribution and geochemical transformations that may impact groundwater quality. Results show that electrical resistivity and phase responses correlate well with dissolved CO_2 injection processes. Specifically, resistivity initially decreases due to increase of bicarbonate and dissolved species. As pH continues to decrease, the resistivity rebounds toward initial conditions due to the transition of bicarbonate into non-dissociated carbonic acid, which reduces the total concentration of dissociated species and thus the water conductivity. An electrical phase decrease is also observed, which is interpreted to be driven by the decrease of surface charge density as well as potential mineral dissolution and ion exchange. Both laboratory and field experiments demonstrate the potential of field complex resistivity method for remotely monitoring changes in groundwater quality due to CO_2 leakage.

1. INTRODUCTION

Geologic carbon sequestration, which aims to capture and inject carbon dioxide (CO_2) into deep subsurface rock formations for long-term storage, is being explored as an avenue toward mitigating the impact of CO_2 emissions on global climate and human health (1). Although the risk of CO_2 leakage from a properly permitted storage reservoir into shallow formations is expected to be very low, assessment and understanding of possible impact of CO_2 leakage is crucial as it could impact groundwater resources. One negative consequence of CO_2 leakage, besides possible brine contamination and release of gaseous CO_2, is a significant increase of dissolved CO_2 into shallow groundwater systems, which will decrease groundwater pH and can potentially mobilize naturally occurring trace metals and ions that are commonly absorbed to or contained in sediments (e.g., 2-5).

Assessing and understanding the potential impact of CO_2 leakage into shallower groundwater systems requires the development of an adequate monitoring strategy to observe dissolved CO_2 plume dynamics and possible geochemical transformations in the subsurface. In the last decade, geophysical methods have demonstrated a significant potential for monitoring hydrological and biogeochemical processes in the shallow subsurface (e.g., 6-8) by complementing direct point measurements, which are usually sparse and thus often have limitations in capturing the three-dimensional (3D) spatial variability of properties and processes. Time-lapse surface and wellbore-based seismic (9-10) and electrical (11) methods, as well as gravimetric and electromagnetic approaches (e.g., 12), have been successfully used to monitor the distribution of the injected CO_2 plume in deep storage reservoirs. Together, these studies document the value of geophysical methods for monitoring an injected CO_2 plume in the deeper reservoir and the need for more spatially extensive approaches for monitoring possible CO_2-induced transformations in

shallower aquifers in case a leak occurs. Although several geophysical methods have demonstrated potential for characterizing hydrological processes in shallow aquifers (such as ground penetrating radar or electrical methods; e.g., 13-17), we are not aware of any studies that have explored the use of geophysical methods for monitoring geochemical impacts of dissolved CO_2.

Here, we evaluate the sensitivity of complex resistivity methods (e.g., 18-19) for monitoring the spatiotemporal distribution of a CO_2 saturated groundwater plume and induced geochemical transformations, including ion exchange and dissolution/precipitation processes, which may impact water quality. Our research is performed using laboratory and field experiments, which both involve (a) the injection of groundwater with dissolved CO_2 into saturated sediments and (b) observation of its impact on water quality and complex resistivity responses. The laboratory experiment permits controlled manipulation under relatively uniform physical heterogeneity (yet with field site materials) and ideal geophysical data acquisition conditions, whereas the field experiments permit assessment of the geophysical methodology over large regions and under naturally heterogeneous and sub-optimal acquisition conditions. The field experiment, which was performed at Plant Daniel about 24 km north of Pascagoula, in Jackson County, Mississippi, is introduced (e.g., site conditions, experimental setup, and geochemical alterations) in a companion paper in this issue (20). Together, the laboratory and field experiments are expected to be useful for documenting the potential of complex resistivity for monitoring CO_2-induced geochemical transformations in aquifers and for exploring the impact of scale on the geophysical response.

The frequency (ω) dependent complex resistivity, $\rho^*(\omega)$, can be defined in terms of a real, ρ', and an imaginary, ρ'', component or by a resistivity magnitude, $|\rho(\omega)|$ (often referred as bulk resistivity and hereafter as resistivity) and an electrical phase, φ, term:

$$\rho^*(\omega) = \rho(\omega)' + i\,\rho(\omega)'' = |\rho(\omega)|e^{i\varphi(\omega)} \qquad (1)$$

The real term measures the electric conduction behavior of a porous medium and the imaginary term measures the charge polarization occurring at the fluid-mineral interface. For geological media, at low frequencies (<1000 Hertz, Hz) the conduction component is primarily controlled by the charge transport via interconnected pore space, which is influenced by the conductivity of the pore fluid (electrolyte), and the pore geometry (i.e., formation factor) (21). The pore fluid electrical conductivity is strongly proportional to ionic strength variations and thus generally to variations in total dissolved solids (TDS) (e.g., 22-23). The polarization processes that occur near the fluid-mineral interface within the electrical double layer are dominated by a diffusive mechanism associated with ion migration to and from the grain surface, and are influenced by mineralogical composition, specific surface area, particle size distribution, and properties of the electrical double layer such as charge density, mobility and thickness (e.g., 24-26).

CO_2 dissolution in groundwater and potential geochemical transformations are expected to influence complex resistivity measurements in various ways depending on the pH and the amount of dissolved CO_2. For example, for groundwater with an initial pH of 8, carbonic acid formed from CO_2 dissolution will primarily dissociate into proton and bicarbonate (see supporting material, Figure S1), thus increase fluid ionic strength and decrease resistivity. Additional pH decrease below the first dissociation constant of carbonic acid (pK_{a1} at ~ pH 6.37 at 25°C (e.g., 27)) will reverse the dissociation process, thus reduce ionic strength and causes the

resistivity to increase toward baseline conditions. The overall surface charge density on mineral surfaces (and thus polarization behavior) is expected to decrease if the pH decreases toward the point of zero charge of the geological media. In addition, possible mineral dissolution/precipitation and ion exchange processes associated with pH decrease from CO_2 dissolution can also change resistivity and phase signals. In particular, promoted ion exchange and mineral dissolution on clay and iron mineral surfaces are expected to produce significant changes in polarization signals. We note that the release of trace metals, whose concentrations are generally too small (in comparison to other ions) to be directly sensed by the complex resistivity methods, depends on several issues including sediment and water composition, organic matter and reduction oxidation conditions (e.g., 28). In this regard complex electrical methods, which can sense some of these processes and properties (as discussed above), may relate to possible proxy (such as Fe for example) for geophysical monitoring of trace metal dynamics.

The objective of this study was to evaluate the sensitivity of complex resistivity methods for monitoring the spatiotemporal distribution of a CO_2 saturated groundwater plume and induced geochemical transformations. To meet this objective, we i) investigated the phase and resistivity response to such processes at the field and laboratory scales, ii) evaluated the capability and accuracy of the complex resistivity approach to image the spatial distribution of an injected dissolved CO_2 plume and associated dynamics at the field scale, and iii) discussed the benefits and limitations of the complex resistivity approach for monitoring and diagnosing CO_2 leakage into shallower aquifer.

2. MATERIALS AND METHODS

2.1. LABORATORY COLUMN EXPERIMENT

The laboratory column experiment consisted of injecting CO_2-saturated groundwater into sediment materials from the field experiment site (described in Section 2.2) under different hydrostatic pressures and observing geochemical transformations and associated complex resistivity responses. The column (20 centimeters (cm) high and 3.8 cm in diameter) was designed to be able to withstand pressure condition at the target aquifer (~ 4 bars) for field experiments. A hydraulic piston was used to simulate overburden pressure at the target depth and pore pressure was controlled using back pressure regulator. Inline pH and conductivity sensors were installed at both ends of the column and four Ag/AgCl electrodes were installed along the column with 5 cm spacing for complex resistivity measurements. Details of the column design are available in supporting material (Figure S2). Silty sands from the field experiment site were wet packed into the column in an anaerobic chamber to avoid exposure to atmospheric O_2, thus preserving the reducing conditions of the material. CO_2 was pre-dissolved into influent container containing site groundwater before injecting into the sediments. The experiment was carried out step-wise, with pCO_2 increasing from 0.69 to 4.14 bars at 0.69 bar with each step (24 hours per step). Four pore volumes of influent solution were injected for each step. Both influent and effluent samples were collected at the end of each step for geochemical analysis using Inductively Coupled Plasma Mass Spectrometry (ICP-MS, Perkin Elmer).

2.2. FIELD EXPERIMENT

2.2.1. FIELD SITE AND EXPERIMENTAL SETUP

Information about the site conditions, experimental setup, and geochemical alterations is given in a companion paper in this issue (20) and briefly summarized here. The approximately 5.8

meters (m) thick target test interval is composed of fine-grained silty sand with minor clay; it is confined between two thick clay units and is located between about 46.9 to 54.6 m below the ground surface. The pumping well (PW1), the injection well (IW1), and 4 monitoring wells (MW1-MW4; Figure 1) were all screened over 4.57 m in the lower part of the target injection zone. The tops of the screened zones were located at 49.4 m (MW2-4), 46.9 (MW1) and 47.9 (PW1 and IW1) m below ground surface.

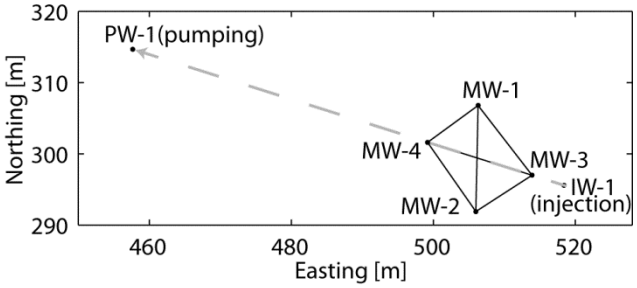

Figure 1. Map view of the field experiment site. Solid black lines indicate profiles where crosshole complex electrical measurements were acquired in a time-lapse mode.

The clay content of the target formation (and other neighboring formations) was estimated using gamma-ray log data (e.g., 29) by normalizing each log by its minimum and maximum measured values, assuming that these extremes are indicative of a pure sand layer and a pure clay layer respectively (e.g., 30). Sampling of the site groundwater prior to injection revealed that the target aquifer had a pH ranging from 7.5 to 8.5 and is dominated by Na^+ and HCO_3^-, with concentrations varying from 140-170 milligrams/Liter (mg/L) and 310-325 mg/L respectively. Water collected before the start of the experiment showed relatively constant major cation (e.g., Mg^{2+}, Ca^{2+}, K^+, and Na^+) and anion (e.g.: Cl^-, HCO_3^-, and SO_4^{2-}) concentrations, with very low trace metal concentrations (20).

The dissolved CO_2 injection experiment was conducted in a dipole setting. Groundwater pumped from PW1 was saturated with CO_2 at the ground surface at a pressure slightly below that of the target aquifer and re-injected into the aquifer (using IW1) in a closed loop to maintain the native redox conditions. Injection of the CO_2 saturated water of pH ~ 5 was initiated on October, 18, 2011 and lasted for about 5 months. Chemical measurements were obtained from water samples collected at the MW1-MW4 wells, which were equipped with dedicated QED bladder pumps with the fluid intakes located at the midpoints of the well screen intervals and connected to a closed flow-cell to minimize atmospheric contamination. Field measurements pH, conductivity, oxidation-reduction-potential (ORP), and temperature were performed within the flow-cell using YSI multi-parameter meters, which were calibrated on a daily basis.

2.2.2. FIELD GEOPHYSICAL DATA ACQUISITION AND PROCESSING

An electrode string with 14 electrodes was placed in each of the monitoring well (MW1-4) screened intervals prior to the experiment. The electrode strings were kept in place until near the end of the injection. The vertical electrode spacing in the wells was 0.35 m and thus the electrode string covered a depth interval of 4.55 m in each of the monitoring wells. It is important to note that the wellbore installation and associated screened zone within each well was determined prior to considering the use of complex resistivity to monitor geochemical transformations associated with the injected CO_2. Given that the well separations ranged from 9.4 to 15.4 m, the limited depth interval covered by the electrodes yields a small aspect ratio (length of screened interval: wellbore spacing) for electrical resistivity imaging (e.g., 18, 31). As such, data acquisition is sub-optimal and imaging from the data is challenging.

Acquisition of electrical measurements was performed by injecting alternating current through two electrodes and measuring the potential difference (voltage) signal between two other electrodes. The complex resistivity data were acquired over multiple frequencies using a DAS-1 multi-channel acquisition system that was set up to be controlled and accessed remotely. The autonomous system was programmed to initiate acquisition automatically almost every night; every other night a reciprocal dataset was also collected. The data were acquired with bipole-bipole and dipole-dipole electrode configurations between each set of wellpairs involving MW1 through MW4 (Figure 1). Assuming a uniform half-space, the apparent resistivity can be inferred from the injected current and the measured potential difference to give a first (pre-inversion) assessment of the dataset. The phase shift of the measured voltage relative to the injected alternating current can also be assessed (e.g., 18-19). Under the steady hydrological and chemical conditions that prevailed prior to CO_2 injection, the average variability between consecutively measured apparent resistivity and repeated and reciprocal values was smaller than 0.08% and 0.7% respectively, while averaged variability between consecutively measured phase and repeated and reciprocal measurements was smaller than 2.5% and 11% respectively. These values indicate reliable measurements although not indicative of the limitations for electrical resistivity imaging in the central part of the profile related to the here sub-optimal aspect ratio in well-bore geometry.

Inverse methods are required to estimate spatial distribution of the electrical properties of the subsurface that reproduce in a given range of uncertainty the measured complex resistivity data that are not related to a specific location but to a complex sensitivity pattern. We inverted the data using CRTomo (32). CRTomo is a smoothness-constraint inversion code that is based on a finite-element algorithm; it solves directly for resistivity and phase within a two-dimensional

(2D) represented region of interest. Inversions of time-lapse data were performed by using the results of a baseline inversion model as the prior model for the subsequent inversion and applying additional constraints that imply minimization of the misfit in a given range of uncertainty and the variation from the baseline model. A larger lateral than vertical smoothing constraint was applied (based on prior lithological information) to stabilize the inversion process.

3. RESULT AND DISCUSSION

3.1. LABORATORY EXPERIMENT RESULTS

Inline sensors revealed a decrease in pH and fluid resistivity during injection of dissolved CO_2 (Figures 2a and 2b). The measured fluid resistivity decreased quite significantly with the injection of dissolved CO_2 at 0.69 bar , which is interpreted to be associated with the increase in ionic strength of the pore fluid due to CO_2 dissolution as discussed above (Figure 2a). This initial decrease of fluid resistivity is followed by a slight rebound because of the transition of bicarbonate into non-dissociated carbonic acid at higher partial CO_2 pressure (pCO_2) conditions (lower pH), which slightly reduced the total concentration of dissociated species as described earlier. The measured resistivity (Figure 2b) shows similar trend than the fluid resistivity but with a rebound occurring at higher pCO_2 conditions (lower pH), which is likely due to its sensitivity to variations in pore structure and not only to fluid resistivity. The more continuous decrease observed in the phase response to 2.07 bars pCO_2 (Figure 2c) is interpreted to be driven by the decrease of surface charge density, which we interpret to be due to the decrease of pH approaching the point of zero charge of silica sand dominant sediments shown to occur at $pH < 4$ (33); the good correlation between electrical phase signal and pH (Figure 2b) support this assumption. An inverse correlation between the phase response and effluent Fe concentration

(Figure 2c) is also observed, which indicates the possible contribution of iron mineral surface and the dissolution and adsorption/desorption process at surface iron sites to the electrical properties of the sample. The decrease of iron concentrations in the later stage may be related to depletion of leachable iron minerals in the sediments.

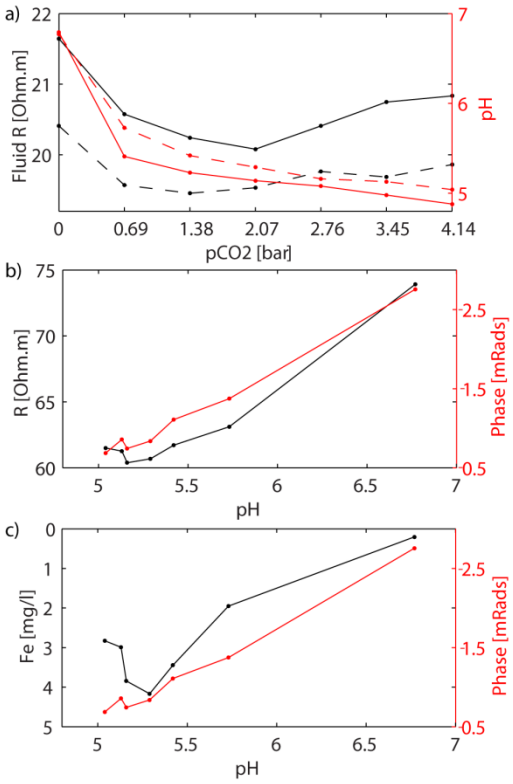

Figure 2. a) measured influent (continuous line) and effluent (dashed line) fluid resistivity and pH during the column experiment involving injection of dissolved CO_2 at various pressure conditions; b) resistivity and phase measured along the column versus the measured pH at the effluent, with c) the phase compared to the Fe concentration at the effluent.

3.2. FIELD EXPERIMENT RESULTS

We consider here the complex resistivity data collected over time between wells MW3 and MW2 (Figure 1) because this profile is located closest to the injection well. In addition, this

transect has the most extensive data set associated with the passage of the plume as well as the most favorable aspect ratio between covered depth interval and distance between the two wells of any of the well pairs. Resistivity inversions were performed between these two wells using about 1150 dipole-dipole and bipole-bipole measurements. The obtained mean absolute difference between the calculated and measured data for each inversion was between 2.4 and 2.9 %. Figure 3 shows the single baseline resistivity image (Figure 3a), as well as the resistivity difference images relative to the baseline, including 12 of the 84 total number of datasets (Figures 3b-3m), which span 7 to 131 days post initiation of CO_2 injection.

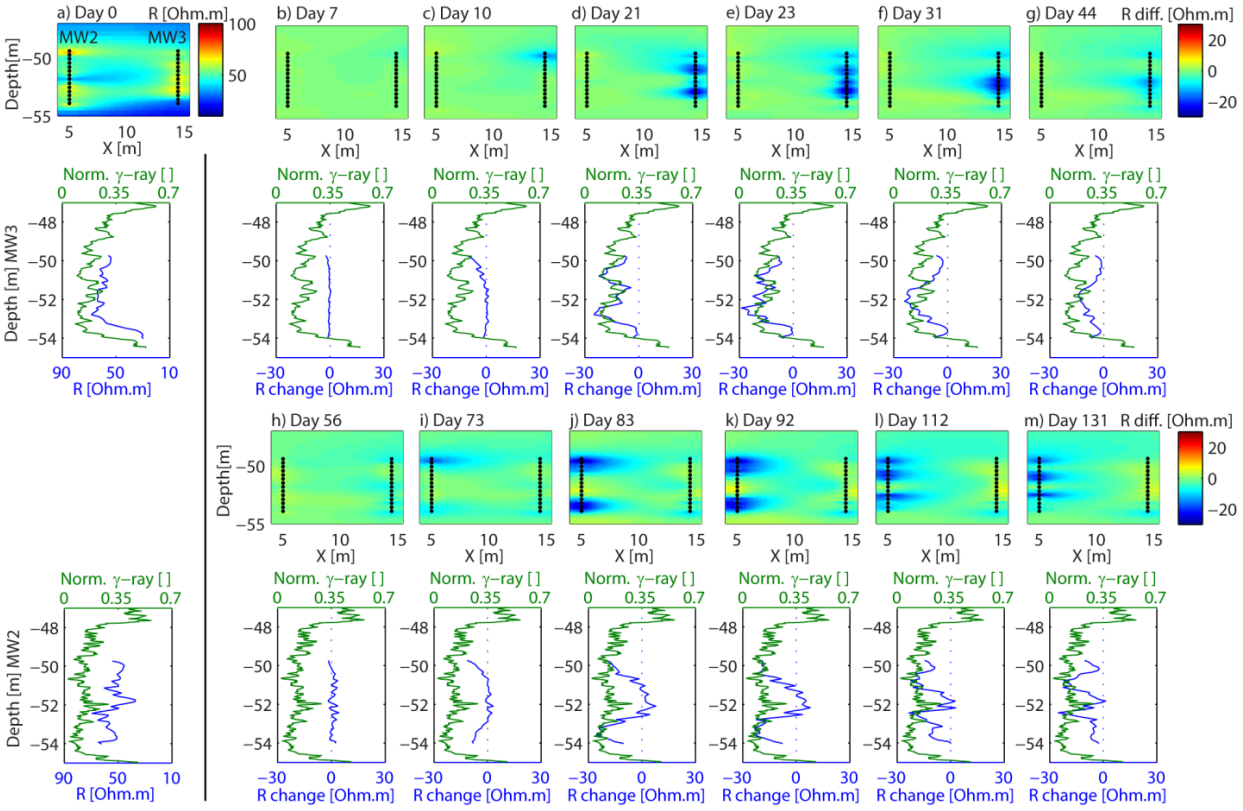

Figure 3. Crosshole resistivity a) inversion between MW2 and MW3 before the start of the experiment (baseline) and b-m) difference along the same profile at various times (negative difference implies smaller resistivity relative to the baseline dataset). The black dots indicate the

electrodes in the wells. Below the tomograms, the imaged resistivity values along MW3 (b-g) and along MW2 (h-m) are compared with the normalized gamma (γ)-logs, which are indicative of the clay content.

The difference images reveal that the first decrease in resistivity occurred near MW3, which is the closest monitoring borehole to the injection well (Figure 1). The decrease in resistivity at MW3 was first evident at the top of the target formation (Figure 3b and c) and then at deeper depths (Figure 3d and e). Over time, the decrease in resistivity became evident in the middle depths at MW3 but rebounded in the upper and lower regions (Figure 3f and g). Approximately 65 days into CO_2 injection, resistivity values near the upper part of MW2 began to decrease (Figure 3i). Because MW2 is the second closest to the injection well after MW3, it makes sense that the impact of the CO_2 plume is detected at this well later in time. With additional time, the resistivity decrease became evident in other parts of the MW2 screened interval (Figure 3j-m). The electrical resistivity decreases and rebounds near MW2 are similar to those observed near MW3, although they happen later in time at MW2 and occur more slowly relative to MW3. The difference in duration of the resistivity decrease-rebound between the two wells confirms that the leading front of the CO_2 plume, which reached MW3 first, spreads over time due to dispersion and heterogeneity. While the resistivity decreases near both wells are consistent with those observed in the laboratory experiments (where a 15-20% decrease was observed) the field-imaged rebounds of resistivity were more significant than those observed in the lab. Although this could be related to differences in the buffering capacity of the sediment and groundwater between lab and field and/or difficulty of replicating field conditions using laboratory columns, further investigation is warranted. In contrast to the nicely imaged decreases in resistivity over time near the wellbore locations, no significant variations were visible in the central part of the

profile (Figure 3h). This is expected as there is lack of sensitivity of the electrical measurements in the inter-wellbore region due to the poor aspect ratio.

The variations in baseline resistivity near the wells correlate well with the heterogeneity indicated by the clay content values inferred from the gamma-logs (Figure 3a). Importantly, changes associated with the CO_2 injection preferentially occurred first in the lower clay content (more permeable zones), which were followed over time by decreases in resistivity where the clay content is higher (or where the permeability is lower) (Figure 3b-m). These results demonstrate both the control of heterogeneity on the CO_2 plume migration and the potential of electrical methods for tracking spatiotemporal variations in geochemical transformations associated with the dissolved CO_2 plume in the presence of natural heterogeneity.

Figure 4 shows the comparison of pH, fluid resistivity and Fe content measured in water samples over time in MW3 and MW2 with the resistivity differences at individual locations within the screened zone extracted from the inverted profiles (Figure 3). The MW3 fluid measurements reveal the arrival of the injected dissolved CO_2 plume about 8 days after the beginning of the injection experiment (Figure 4a) as indicated by a decrease in pH followed shortly thereafter by a decrease in water resistivity and increase in Fe concentration. This pH decrease toward the pH of the injected CO_2 saturated water indicates the presence of more and more dissolved CO_2 and an increasing ratio between moles of non-dissociated carbonic acid and bicarbonate (Figure S1). After about 23 days of continuous injection, the fluid resistivity change that is known to be (negatively) correlated with TDS change (e.g., 22-23) rebounded toward background values although the pH remained low. Similar trend is followed by the total alkalinity, and the concentrations of ions (e.g., Ca, Na, Mg, K) and trace metals (e.g., Ba, Fe, Sr, Mn) (detailed geochemistry not shown) (20), which all increase toward a peak value until the pH

approaches ~5.6 and then decreased as the pH continued to slightly decrease. Similar early-time geochemical responses were observed in Well MW2, where the injected dissolved CO_2 plume started to become visible in water samples at ~65 days after the start of the injection (Figure 4b).

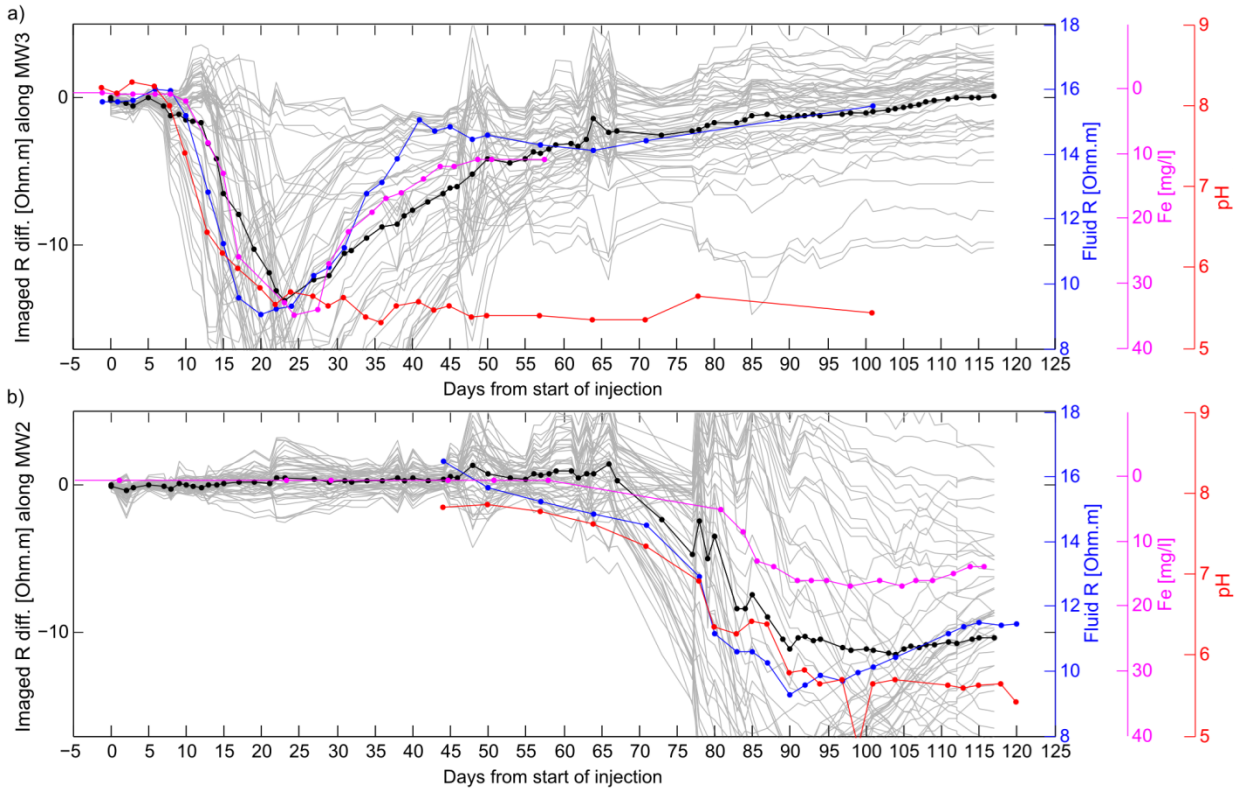

Figure 4. Comparison between pH, Fe, fluid resistivity from water samples with changes in resistivity extracted from tomograms (Figure 3) in a) MW3 and b) MW2. The grey lines show the resistivity difference estimates associated with individual depth locations within the screened zone, while the black line shows the averaged resistivity difference over the entire interval.

The measured fluid resistivity and Fe concentrations variations compare well with the averaged resistivity difference along MW3 and MW2, all showing similar behaviors and shape, although some differences exist likely due to various sampled volume, location and averaging

process (Figure 4). Importantly, the imaged resistivity variations at various depths along MW2 and MW3 (grey lines in Figure 4) illustrate the vertical variability in the arrival of the plume, which is not assessed from the depth-averaged water samples alone.

The challenging acquisition geometry did not permit a successful inversion of the 2D phase response. However, phase measurements do show some coherent near-wellbore variations over time, which can be observed through assessing the measured phase acquired when the four electrodes are located in a single wellbore. For example, Figure 5 shows the near wellbore phase response over time when electrodes having 0.7 m vertical interval spacing are located in MW3. The measured phase variations show a similar decrease than the resistivity with the arrival of the plume but a much smaller rebound at later time. This is consistent with the results of the laboratory experiment, which indicate also a much more limited rebound in phase due to the decrease of surface charge density that is maintained while the plume is present. These results demonstrate the significant potential of monitoring the phase variations that are indicative of the presence of the plume and provide complementary (and not redundant) information to the resistivity measurements, which are here not sensitive to plume variations once the pH is very low.

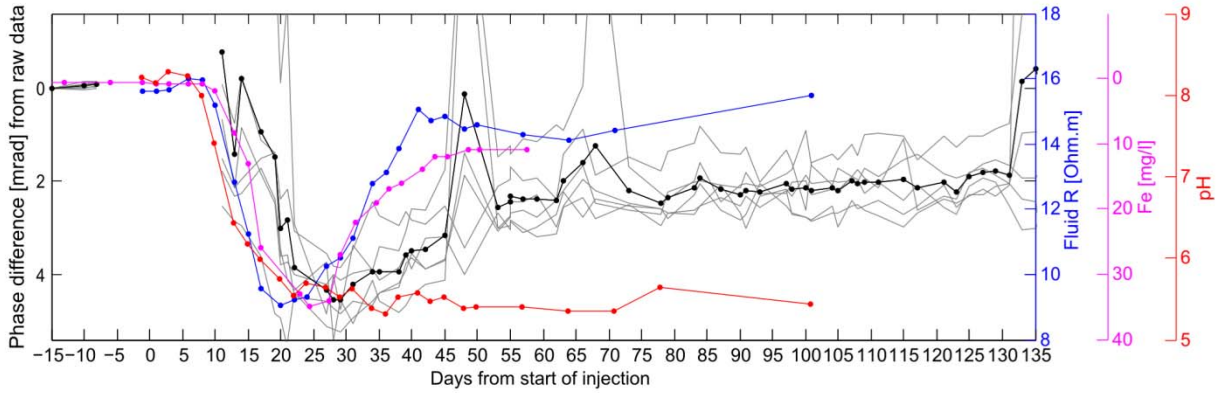

Figure 5. Comparison in MW3 between pH, Fe, fluid resistivity from water samples with phase variations in the measured raw geophysical data. The grey lines show phase variations associated with electrodes at different depths, while the black line shows the average (positive difference implies decrease toward zero from the baseline measured negative phases).

3.3 DISCUSSION

The results of this study demonstrate the potential of complex electrical time-lapse surveys for remotely monitoring the spatiotemporal distribution of dissolved CO_2 plumes and their associated geochemical transformations. Laboratory and field experiments consistently indicated that electrical resistivity and phase measurements reliably responded to variations in fluid conductivity and polarization at the fluid-mineral interface caused by geochemical changes induced by the injected dissolved CO_2. Specifically, a progressive increase of the amount of dissolved CO_2 in groundwater initially led to a resistivity decrease due to increase of bicarbonate and dissolved species; this decrease was followed by a rebound associated with the continued lowering of pH and related transition of bicarbonate into non-dissociated carbonic acid, which reduced the total concentration of dissociated species. An electrical phase decrease was also observed, and is related to the decrease of surface charge density driven by the decrease of pH approaching the point of zero charge of silica sand dominant sediments. Phase decrease is also related to mineral dissolution and ion exchange processes at the mineral surface, iron in particular at low pH. Ongoing research focuses on distinguishing the effects of mineral dissolution and ion exchange on polarization from those associated with a pH decrease. These results indicate the potential for monitoring dissolved CO2 with i) resistivity to detect and image variations in ionic strength and thus key ion concentration due to CO2 dissolution, which is crucial for water quality monitoring and ii) phase to sense plume-induced alteration of minerals

and pH dependant polarization and thus continue to detect the plume after the front of the plume passed. Complex resistivity methods have shown also the potential in being used as a proxy for monitoring geochemical transformations and possible variations in trace elements concentrations, which is crucial for water quality monitoring.

Our study has shown that the complex electrical autonomous monitoring strategy is very robust with regard to repeatability of the measurements and sensitivity to geochemically-induced resistivity variations in the surveyed region. Relevant variations in apparent resistivity lower than one percent can be detected in the raw data, which can easily be distinguished from random noise by assessing continuous variations and from very local disturbances through the consideration of measurements collected from different acquisition configurations.

In addition the presented strategy provides additional information to well measurements about the plume distribution and related geochemical transformation in the presence of heterogeneity, which is essential for improving hydrological and geochemical field parameter estimation. It may also be useful for reducing the cost of wellbore chemical sampling and for understanding the information content of wellbore measurements, which often reflect some averaged conditions over the length of a well screen. Our results also suggest that the complex resistivity variations can provide information about the presence of a plume before it can be detected through well water sample analysis. Additionally, with more favorable wellbore geometry, we would anticipate more effective 2D imaging.

In summary, our coupled laboratory and field studies indicate the potential of the complex resistivity method for remotely monitoring and detecting dissolved CO_2 induced geochemical transformations in case a CO_2 leak occurs. The results of this first attempt to use this method as a monitoring approach are promising; synthetic studies are underway to explore the extension of

this method for monitoring larger scale regions where prior knowledge about leak location is not available. To enable covering large regions with an acceptable cost, such monitoring may require that the method be deployed using a combination of complex resistivity crosshole and surface-based acquisition geometries, with possible addition of surface and airborne electromagnetic measurements. One persisting challenge is imaging variations from the surface that occur at deep depths and below thick confining layers. Importantly, a dissolved CO_2 plume is expected to migrate and expand laterally as governed by the hydrological flow gradient and thus acquisition geometry needs to be adapted to the hydrological system. Also laboratory studies are worth to evaluate/recognize possible chemical processes (which may be very site dependent) and complex resistivity signature. In spite of these challenges, the results presented here suggest that extension of the method to larger scale is warranted and holds potential to provide prompt and accurate detection of the spatiotemporal distribution of leaked CO_2 and associated geochemical transformations over field relevant scales, as is needed for environment risk assessment.

ACKNOWLEDGMENTS

This work was funded by the Assistant Secretary for Fossil Energy, National Energy Technology Laboratory (NETL), National Risk Assessment Program (NRAP), of the US Department of Energy under Contract No. DE-AC02-05CH11231, in collaboration with the Electric Power Research Institute. We thank Dr. A. Kemna and M. Weigand at University of Bonn for providing the 2D complex resistivity imaging code.

SUPPORTING INFORMATION AVAILABLE

Supporting information includes a schematic view of the carbonate species distribution as a function of pH and injected dissolved CO_2 (Figure S1) and a schematic view of the laboratory column experiment (Figure S2).

REFERENCES

(1) IPCC *Special report on carbon dioxide capture and storage*; B. Metz, O., Davidson, H. C. de Coninck, M. Loos, L. A. Meyer, Eds., Intergovernmental Panel on Climate Change: 2006; p 440.

(2) Kharaka, Y. K.; Thordsen, J. J.; Kakouros, E.; Ambats, G.; Herkelrath, W. N.; Beers, S. R.; Birkholzer, J. T.; Apps, J. A.; Spycher, N. F.; Zheng, L.; Trautz, R. C.; Rauch, H. W.; Gullickson, K. S., Changes in the chemistry of shallow groundwater related to the 2008 injection of CO_2 at the ZERT field site, Bozeman, Montana. *Environmental Earth Sciences* **2010,** *60* (2), 273-284.

(3) Little, M. G.; Jackson, R. B., Potential impacts of leakage from deep CO_2 geosequestration on overlying freshwater aquifers. *Environmental Science & Technology* **2010,** *44* (23), 9225-9232.

(4) Peter, A.; G., H.; Beyer, M.; Lamert, H.; Heinrich, B.; Geistlinger, H. W.; Werban, U.; Dietrich, P.; Grossmann, J.; Garbe-Schoenberg, C. D.; Dahmke, A., Geochemical alteration of shallow groundwater due to injection of CO_2. *Paper Presented at the American Geophysical Union Fall Meeting*, San Francisco, USA, 2011; Vol. Abstract H42C-06.

(5) Zheng, L.; Apps, J. A.; Spycher, N.; Birkholzer, J. T.; Kharaka, Y. K.; Thordsen, J.; Beers, S. R.; Herkelrath, W. N.; Kakouros, E.; Trautz, R. C., Geochemical modeling of changes in shallow groundwater chemistry observed during the MSU-ZERT CO_2 injection experiment. *International Journal of Greenhouse Gas Control* **2012,** *7*, 202-217.

(6) Atekwana, E. A.; Slater, L. D., Biogeophysics: A New Frontier in Earth Science Research. *Reviews of Geophysics* **2009,** *47*.

(7) Hubbard, S. S.; Rubin, Y., Introduction to hydrogeophysics. In *Hydrogeophysics*, Rubin, Y.; Hubbard, S. S., Eds. Springer: Dordrecht, The Netherlands, 2005; pp 3-21.

(8) Vereecken, H.; Binley, A.; Cassiani, G.; Revil, A.; Titov, K., *Applied Hydrogeophysics* Springer: 2006; p 395.

(9) Chadwick, R. A.; Noy, D.; Arts, R.; Eiken, O., Latest time-lapse seismic data from Sleipner yield new insights into CO_2 plume development. *Energy Procedia* **2009,** *1* (1), 2103-2110.

(10) Daley, T. M.; Myer, L. R.; Peterson, J. E.; Majer, E. L.; Hoversten, G. M., Time-lapse crosswell seismic and VSP monitoring of injected CO_2 in a brine aquifer. *Environmental Geology* **2008,** *54* (8), 1657-1665.

(11) Kiessling, D.; Schmidt-Hattenberger, C.; Schuett, H.; Schilling, F.; Krueger, K.; Schoebel, B.; Danckwardt, E.; Kummerow, J.; Grp, C. S., Geoelectrical methods for monitoring geological CO_2 storage: First results from cross-hole and surface-downhole measurements from the CO_2SINK test site at Ketzin (Germany). *International Journal of Greenhouse Gas Control* **2010,** *4* (5), 816-826.

(12) JafarGandomi, A.; Curtis, A., Detectability of petrophysical properties of subsurface CO_2-saturated aquifer reservoirs using surface geophysical methods. *Leading Edge* **2011,** *30* (10).

(13) Hyndman, D. W.; Gorelick, S. M., Estimating lithologic and transport properties in three dimensions using seismic and tracer data: The Kesterson aquifer. *Water Resources Research* **1996,** *32* (9), 2659-2670.

(14) Hubbard, S. S.; Rubin, Y.; Majer, E., Ground-penetrating-radar-assisted saturation and permeability estimation in bimodal systems. *Water Resources Research* **1997,** *33* (5), 971-990.

(15) Johnson, T. C.; Versteeg, R. J.; Huang, H.; Routh, P. S., Data-domain correlation approach for joint hydrogeologic inversion of time-lapse hydrogeologic and geophysical data. *Geophysics* **2009,** *74* (6), F127-F140.

(16) Kowalsky, M. B.; Finsterle, S.; Peterson, J.; Hubbard, S.; Rubin, Y.; Majer, E.; Ward, A.; Gee, G., Estimation of field-scale soil hydraulic and dielectric parameters through joint inversion of GPR and hydrological data. *Water Resources Research* **2005,** *41* (11), W11425.

(17) Singha, K.; Gorelick, S. M., Saline tracer visualized with three-dimensional electrical resistivity tomography: Field-scale spatial moment analysis. *Water Resources Research* **2005,** *41* (5), W05023.

(18) Binley, A.; Kemna, A., DC Resistivity and induced Polarization Methods. In *Hydrogeophysics*, Rubin, Y.; Hubbard, S. S., Eds. Springer: 2005; pp 129-156.

(19) Slater, L.; Lesmes, D. P., Electrical-hydraulic relationships observed for unconsolidated sediments. *Water Resources Research* **2002,** *38* (10), 1213.

(20) Trautz, R. C.; Pugh, J. D.; Varadharajan, C.; Zheng, L.; Bianchi, M.; Nico, P. S.; Spycher, N. F.; Newell, D. L.; Birkholzer, J. T.; Esposito, R. A.; Wu, Y.; Dafflon, B.; Hubbard, S. S., Effect of a controlled release of dissolved CO_2 on a shallow groundwater system. *Environ. Sci and Tech* **submitted**.

(21) Archie, G. E., The electrical resistivity log as an aid in determining some reservoir characteristics. *Petroleum Transactions of AIME* **1942,** *146*, 54-62.

(22) Visconti, F.; de Paz, J. M.; Rubio, J. L., An empirical equation to calculate soil solution electrical conductivity at 25 degrees C from major ion concentrations. *European Journal of Soil Science* **2010,** *61* (6), 980-993.

(23) McCleskey, R. B.; Nordstrom, D. K.; Ryan, J. N.; Ball, J. W., A new method of calculating electrical conductivity with applications to natural waters. *Geochimica et Cosmochimica Acta* **2012,** *77*, 369-382.

(24) Kemna, A.; Binley, A.; Slater, L., Crosshole IP imaging for engineering and environmental applications. *Geophysics* **2004,** *69* (1), 97-107.

(25) Orozco, A. F.; Williams, K. H.; Long, P. E.; Hubbard, S. S.; Kemna, A., Using complex resistivity imaging to infer biogeochemical processes associated with bioremediation of an uranium-contaminated aquifer. *Journal of Geophysical Research-Biogeosciences* **2011,** *116*.

(26) Wu, Y.; Hubbard, S.; Williams, K. H.; Ajo-Franklin, J., On the complex conductivity signatures of calcite precipitation. *Journal of Geophysical Research-Biogeosciences* **2010,** *115*.

(27) Fitts, C. R., *Groundwater Science*. Academic Press: San Diego, California, 2002; p 450.

(28) Tessier, A.; Fortin, D.; Belzile, N.; DeVitre, R. R.; Leppard, G. G., Metal sorption to diagenetic iron and manganese oxyhydroxides and associated organic matter: Narrowing the gap between field and laboratory measurements. *Geochimica et Cosmochimica Acta* **1996,** *60* (3), 387-404.

(29) Serra, O.; Serra, L., *Well Logging: Data Acquisitions and Applications*. Technip Editions: Paris, France, 2004; p 688.

(30) Schön, J. H., *Physical properties of rocks: Fundamentals and principles of Petrophysics*. Elsevier: Oxford, UK, 2004; p 583.

(31) LaBrecque, D. J.; Ramirez, A. L.; Daily, W. D.; Binley, A. M.; Schima, S. A., ERT monitoring on environmental remediation processes. *Measurement Science & Technology* **1996,** *7* (3), 375-383.

(32) Kemna, A. *Tomographic inversion of complex resistivity – theory and application*. Ph.D. thesis, Ruhr University, Bochum 2000.

(33) Kosmulski, M., pH-dependent surface charging and points of zero charge. IV. Update and new approach. *Journal of Colloid and Interface Science* **2009,** *337* (2), 439-448.